

Mapped *spdf* interacting boson model for quadrupole-octupole collective states in nuclei

K. Nomura*

Department of Physics, Hokkaido University, Sapporo 060-0810, Japan and
Nuclear Reaction Data Center, Hokkaido University, Sapporo 060-0810, Japan

(Dated: October 21, 2025)

Dipole bosons are introduced in the interacting boson model (IBM) by means of the self-consistent mean-field method. The constrained mean-field calculations employing a given nuclear energy density functional yield the potential energy surfaces in terms of the axially-symmetric quadrupole-octupole, dipole-quadrupole, and dipole-octupole deformations. By mapping these energy surfaces onto the expectation values of the IBM Hamiltonian in the coherent state of the interacting s , p , d , and f bosons, strength parameters of the *spdf*-IBM Hamiltonian are determined. In an illustrative application to octupole-deformed actinides $^{218-230}\text{Ra}$ and $^{220-232}\text{Th}$, it is shown that effects of including p bosons in the IBM mapping are to lower significantly negative-parity yrast levels, and to improve descriptions of observed energy-level systematic in nearly spherical and transitional nuclei, and of the behaviors of the reduced electric dipole transitions and intrinsic dipole moments with neutron number.

I. INTRODUCTION

Low-lying collective states of most nuclei are dominated by the quadrupole modes including the anharmonic vibrations of the nuclear surface and rotational motions. Higher-order, i.e., octupole, hexadecapole, etc. deformations also arise and come to play a role in determining the low-lying nuclear structure. The octupole collectivity, in particular, corresponds to a reflection asymmetric (or pear-like) deformation, which breaks parity. The octupole modes of collective excitations are characterized by the appearance of negative-parity bands that are close in energy to the positive-parity ground-state bands, forming alternating-parity bands, and by the appreciable electric octupole ($E3$) transitions [1–4].

In fact, nuclides that are known to exhibit a static octupole deformation are rare, the experimental evidence being suggested in a few radioactive nuclei, e.g., ^{220}Rn [5], ^{224}Ra [5], ^{144}Ba [6], and ^{146}Ba [7]. These nuclei correspond to the neutron N and/or proton Z numbers close to 56, 88, 136, at which nucleon numbers a coupling of two single-particle orbits that differ by $\Delta j = \Delta l = 3\hbar$ occurs, with j and l denoting the quantum numbers of a single-particle state. The presence of the octupole correlations also represents a broader physical significance, as it enhances the atomic electric dipole moment (EDM), the observation of which implies violation of time reversal (T) or charge parity (CP) [8]. Theoretical investigations for the quadrupole and octupole deformations and collective excitations have been made in various nuclear structure models (see, e.g., Refs. [2–4, 9, 10] and some related references therein).

The low-lying quadrupole and octupole states have extensively been studied by using the framework of the interacting boson model (IBM) [11]. The IBM comprises the monopole, s , and quadrupole, d , bosons, which

represent the collective monopole (with spin and parity $J^\pi = 0^+$) and quadrupole ($J^\pi = 2^+$) pairs of valence nucleons, respectively [11–13]. In order to compute negative-parity states octupole, f , bosons, representing the collective octupole (with $J^\pi = 3^-$) nucleon pairs, have been introduced [11, 14, 15]. In the last decade, in particular, a method of deriving the *sdf*-IBM Hamiltonian using the framework of the nuclear energy density functional (EDF) theory has been developed [16, 17]. The first step within this scheme is the self-consistent mean-field (SCMF) calculation with constraints on the quadrupole and octupole moments, which is based on a given nuclear EDF, e.g., in the nonrelativistic or relativistic regimes. The self-consistent calculation yields the potential energy surface (PES) defined in the quadrupole and octupole deformations. The next step is to map the PES onto the corresponding energy surface in the *sdf*-boson system, by which procedure the strength parameters of the *sdf*-IBM Hamiltonian are determined. The method, denoted hereafter as the mapped IBM, has been applied to study relevance of octupole correlations in low-energy collective states in sets of medium-heavy and heavy nuclei in different mass regions in which octupole deformations are expected to emerge (see Refs. [18, 19] for reviews). This approach, however, has a difficulty of not being able to reproduce observed electric dipole ($E1$) transition properties even qualitatively, and this deficiency has been attributed to some missing boson degrees of freedom.

Indeed, in the initial implementation of the IBM [14] in the study of reflection asymmetric nuclear states, dipole, p , bosons, with $J^\pi = 1^-$, were considered as a building block in addition to f bosons. However, while from a microscopic point of view d and f bosons can be, as mentioned, interpreted to be collective in nature, the origin of a p boson appears to have been less obviously established. That is, it was attributed either to the spurious center-of-mass motion [15], or to the giant dipole resonance [20]. Mathematically the version of the IBM that includes p

* nomura@sci.hokudai.ac.jp

bosons (denoted *spdf*-IBM) furnishes the group SU(16) [14, 15, 21, 22], and to produce the rotational limit SU(3) the model should contain *f* and *p* bosons. Also in realistic applications, the *spdf*-IBM gives improved descriptions, in particular, of the *E1* properties of the octupole deformed nuclei over the *sdf*-IBM [20, 23–26]. A *p* or dipole boson degree of freedom can also be considered to represent an α particle, and has been introduced to describe molecular-like structures in light [27] and heavy [25, 28, 29] nuclei. In addition, it was shown that the dipole pairs account for the intrinsic state of deformed actinides to a large extent, and should be considered as essential building blocks as the octupole pairs [30, 31]. It appears, therefore, that the IBM model space may need to contain dipole bosons for the calculations of octupole-deformed nuclei, and it is of interest to study *p*-boson effects on various physical observables of these nuclear systems in a timely manner.

In the following, dipole (*p*) bosons are introduced in the aforementioned IBM mapping procedure. Relevance of including *p* bosons to reproducing energy spectra and transition properties of positive-parity and negative-parity collective states is addressed by taking as an illustrative example axially-deformed actinides $^{218-230}\text{Ra}$ and $^{220-232}\text{Th}$. The PESs as the microscopic input are provided by the Hartree-Fock-Bogoliubov (HFB) SCMF calculations [9] employing the finite range, Gogny force [32] with the D1M parametrization [33], performed with constraints on the axial quadrupole, octupole, and dipole moments. In the SCMF framework, the dipole deformation effects on PESs have been discussed in quite a few instances, e.g., Refs. [34–36]. Also geometry of the *spdf*-IBM Hamiltonian was studied in the coherent state framework in Ref. [37]. Here the quadrupole and octupole deformations in the fermionic system are associated with the bosonic counterparts, as has been done previously [10, 16, 17]. By analogy with these associations, the bosonic deformation corresponding to *p* bosons is assumed to represent the electric dipole moment in the fermionic system, which is used as additional collective coordinate in the SCMF calculations. It is noted that the mapped *sdf*-IBM calculations on the above nuclei were made in Ref. [10] using the same microscopic input, i.e., Gogny-D1M EDF. Some of the results reported in that reference are exploited in the present work, that is, the quadrupole-octupole PESs, and derived parameters for the *sdf*-IBM. To identify *p*-boson effects on various physical observables, simpler *sdf*-IBM calculations are also performed, and are compared with the more realistic *spdf*-IBM results.

The theoretical procedure is illustrated in Sec. II. The mapped *spdf*-IBM results for the PESs, derived parameters, spectroscopic properties including excitation energies and transition properties, and detailed energy spectra for a few selected nuclei are given in Sec. III. Summary of the main results and concluding remarks are given in Sec. IV.

II. THEORETICAL PROCEDURE

The procedure starts with the constrained self-consistent calculations of the PESs for $^{218-230}\text{Ra}$ and $^{220-232}\text{Th}$. In Ref. [10] the Gogny-D1M HFB SCMF calculations were made for these nuclei with the constraints on axially symmetric mass quadrupole q_{20} and octupole q_{30} intrinsic moments, with the center-of-mass being fixed at the origin [38, 39]. The q_{20} and q_{30} moments are expressed as the geometrical deformations [40] denoted as β_{20} and β_{30} , respectively:

$$\beta_{\lambda 0} = \frac{\sqrt{(2\lambda + 1)\pi}}{3R_0^\lambda A} q_{\lambda 0} \quad (1)$$

with $R_0 = 1.2A^{1/3}$ fm and $\lambda = 2, 3$. The HFB calculations provided PESs in terms of the β_{20} and β_{30} deformations. In the present work, additional Gogny-D1M HFB calculations are carried out using the computer program HFBTHO (v4.0) [41] that include the axial quadrupole, octupole, and dipole deformations as collective coordinates, and yield two energy surfaces: one in terms of the dipole and quadrupole deformations, and the other of the dipole and octupole deformations. To compute the dipole-quadrupole and dipole-octupole PESs, the remaining deformation (octupole and quadrupole, respectively) is fixed at the value corresponding to the global minimum in the (β_{20}, β_{30}) -PES obtained in Ref. [10]. In what follows the intrinsic dipole deformation is conveniently expressed by the symbol β_{10} , which is obtained by using the formula of Eq. (1) with $\lambda = 1$, as in the case of the quadrupole and octupole deformations. Also the $\beta_{\lambda 0}$ deformations are denoted simply as β_λ .

The HFB (β_2, β_3) -, (β_1, β_2) -, and (β_1, β_3) -PESs thus obtained for each nucleus are associated with the bosonic counterparts in the *spdf*-IBM. The *spdf*-IBM Hamiltonian adopted in the present study reads

$$\hat{H}_B = \epsilon_d \hat{n}_d + \epsilon_f \hat{n}_f + \epsilon_p \hat{n}_p + \kappa_2 \hat{Q} \cdot \hat{Q} + \kappa_3 \hat{O} \cdot \hat{O} + \kappa_1 \hat{D} \cdot \hat{D} + \kappa' \hat{L} \cdot \hat{L}. \quad (2)$$

The first, second, and third terms denote the single *d*, *f*, and *p* boson number operators, and are given as $\hat{n}_d = d^\dagger \cdot \tilde{d}$, $\hat{n}_f = f^\dagger \cdot \tilde{f}$, and $\hat{n}_p = p^\dagger \cdot \tilde{p}$, respectively, with ϵ_d , ϵ_f , ϵ_p representing the single *d*, *f*, and *p* boson energies relative to that of an *s* boson. Note the notations $\tilde{d}_\mu = (-1)^\mu d_{-\mu}$, $\tilde{f}_\mu = (-1)^{3+\mu} f_{-\mu}$, and $\tilde{p}_\mu = (-1)^{1+\mu} p_{-\mu}$. The fourth, fifth, and sixth terms in (2) stand for quadrupole-quadrupole, octupole-octupole, and dipole-dipole interactions, respectively, with the corresponding strength parameters κ_2 , κ_3 , and κ_1 . The quadrupole \hat{Q} , octupole \hat{O} , and dipole \hat{D} operators read

$$\hat{Q} = s^\dagger \tilde{d} + d^\dagger s + \chi_{dd} (d^\dagger \times \tilde{d})^{(2)} + \chi_{pp} (p^\dagger \times \tilde{p})^{(2)} + \chi_{pf} (p^\dagger \times \tilde{f} + f^\dagger \times \tilde{p})^{(2)} + \chi_{ff} (f^\dagger \times \tilde{f})^{(2)}, \quad (3)$$

$$\hat{O} = s^\dagger \tilde{f} + f^\dagger s + \chi_{pd} (p^\dagger \times \tilde{d} + d^\dagger \times \tilde{p})^{(3)} + \chi_{df} (d^\dagger \times \tilde{f} + f^\dagger \times \tilde{d})^{(3)}, \quad (4)$$

$$\hat{D} = s^\dagger \tilde{p} + p^\dagger s + \chi'_{pd}(p^\dagger \times \tilde{d} + d^\dagger \times \tilde{p})^{(1)} + \chi'_{df}(d^\dagger \times \tilde{f} + f^\dagger \times \tilde{d})^{(1)}, \quad (5)$$

with χ s being dimensionless parameters. The last term in Eq. (2), with \hat{L} being the boson angular momentum operator

$$\hat{L} = \sqrt{10}(d^\dagger \times \tilde{d})^{(1)} - \sqrt{28}(f^\dagger \times \tilde{f})^{(1)}, \quad (6)$$

is introduced because it plays an important role in describing moments of inertia of rotational bands in axially deformed nuclei as those considered in this study. In addition, as in previous mapped *sdf*-IBM studies the term proportional to $(d^\dagger \times \tilde{d})^{(1)} \cdot (f^\dagger \times \tilde{f})^{(1)}$, arising in the product $\hat{L} \cdot \hat{L}$ is omitted for simplicity.

The energy surface is obtained in terms of the three deformations $(\beta_1, \beta_2, \beta_3)$ as the expectation value of the *sdf*-IBM Hamiltonian (2):

$$E_{\text{IBM}}(\beta_1, \beta_2, \beta_3) = \frac{\langle \phi(\beta_1, \beta_2, \beta_3) | \hat{H}_{\text{B}} | \phi(\beta_1, \beta_2, \beta_3) \rangle}{\langle \phi(\beta_1, \beta_2, \beta_3) | \phi(\beta_1, \beta_2, \beta_3) \rangle}. \quad (7)$$

Here the ket $|\phi(\beta_1, \beta_2, \beta_3)\rangle$ represents the coherent state [42] of s , p , d , and f bosons, and is given by

$$|\phi(\beta_1, \beta_2, \beta_3)\rangle = \frac{1}{\sqrt{n!}} (\lambda^\dagger)^n |0\rangle, \quad (8)$$

where $|0\rangle$ and n represents the inert core, and the number of bosons, respectively, and

$$\lambda^\dagger = s^\dagger + \bar{\beta}_1 p_0^\dagger + \bar{\beta}_2 d_0^\dagger + \bar{\beta}_3 f_0^\dagger. \quad (9)$$

$\bar{\beta}_\lambda$ stand for the boson analogs of the dipole, quadrupole, and octupole deformations. As conventionally made, the bosonic deformations for each value of λ are assumed to be proportional to the fermionic deformations [16, 42, 43], i.e.,

$$\bar{\beta}_\lambda = C_\lambda \beta_\lambda. \quad (10)$$

The proportionality constants C_λ are usually larger than unity, that is, the bosonic deformation is larger than the fermionic deformation. This accounts for the fact that the IBM space is comprised only of a limited number of valence nucleons, whereas in the present HFB all constituent nucleons are involved. The energy surface $E_{\text{IBM}}(\beta_1, \beta_2, \beta_3)$ is obtained as the following analytical expression:

$$E_{\text{IBM}}(\beta_1, \beta_2, \beta_3) = \frac{n}{1 + \bar{\beta}_1^2 + \bar{\beta}_2^2 + \bar{\beta}_3^2} (\epsilon'_s + \epsilon'_p \bar{\beta}_1^2 + \epsilon'_d \bar{\beta}_2^2 + \epsilon'_f \bar{\beta}_3^2) + \frac{n(n-1)}{(1 + \bar{\beta}_1^2 + \bar{\beta}_2^2 + \bar{\beta}_3^2)^2} \times \left[\kappa_2 \left(2\bar{\beta}_2 - \sqrt{\frac{2}{7}} \chi_{dd} \bar{\beta}_2^2 + \sqrt{\frac{2}{3}} \chi_{pp} \bar{\beta}_1^2 - 2\sqrt{\frac{3}{7}} \chi_{pf} \bar{\beta}_1 \bar{\beta}_3 + \frac{2}{\sqrt{21}} \chi_{ff} \bar{\beta}_3^2 \right)^2 + 4\kappa_3 \left(\bar{\beta}_3 + \sqrt{\frac{3}{5}} \chi_{pd} \bar{\beta}_1 \bar{\beta}_2 - \frac{2}{\sqrt{15}} \chi_{df} \bar{\beta}_2 \bar{\beta}_3 \right)^2 + 4\kappa_1 \left(\bar{\beta}_1 - \sqrt{\frac{2}{5}} \chi'_{pd} \bar{\beta}_1 \bar{\beta}_2 + \frac{3}{\sqrt{35}} \chi'_{df} \bar{\beta}_2 \bar{\beta}_3 \right)^2 \right]. \quad (11)$$

Note that ϵ' s in the above formula arise from contractions made when calculating the expectation values of two-

body boson terms, and are defined as

$$\begin{aligned} \epsilon'_s &= 5\kappa_2 - 7\kappa_3 - 3\kappa_1 \\ \epsilon'_d &= \epsilon_d + 6\kappa' + (1 + \chi_{dd}^2) \kappa_2 \\ &\quad + \frac{7}{5} \kappa_3 (\chi_{pd}^2 + \chi_{df}^2) + \frac{3}{5} \kappa_1 (\chi_{pd}'^2 + \chi_{df}'^2) \\ \epsilon'_f &= -\epsilon_f + 12\kappa' + \frac{5}{7} \kappa_2 (\chi_{ff}^2 + \chi_{pf}^2) \\ &\quad + (1 + \chi_{df}^2) \kappa_3 + \frac{3}{7} \kappa_1 \chi_{df}'^2 \\ \epsilon'_p &= -\epsilon_p + \frac{5}{3} \kappa_2 (\chi_{pp}^2 + \chi_{pf}^2) + (1 + \chi_{pd}'^2) \kappa_1 + \frac{7}{3} \kappa_3 \chi_{df}^2. \end{aligned} \quad (12)$$

The procedure to determine the parameters that ap-

pear in (11) including the coefficients C_λ is summarized as follows.

- (i) The HFB-to-IBM mapping is carried out in the (β_2, β_3) -deformation space with $\beta_1 = 0$. First, the parameters $(\epsilon_d, \kappa_2, \chi_{dd}, C_2)$, which are related to sd bosons, are obtained by reproducing the topology near the minimum of the HFB PES along the $\beta_3 = 0$ axis, that is, the deformation at which the minimum occurs, depth and steepness of the potential valley, should be reasonably reproduced. Since the $\hat{L} \cdot \hat{L}$ term does not make a unique contribution to the energy surface, the strength κ' has to be determined separately in such a way [44] that the cranking moment of inertia calculated in the intrinsic state of the sd -boson system at the minimum on the $\beta_3 = 0$ axis should be equal to the Thouless-Valatin moment of inertia [45] calculated by the HFB.
- (ii) Second, the parameters that are related to f bosons (or octupole deformation), i.e., $(\epsilon_f, \chi_{ff}, \kappa_3, \chi_{df}, C_3)$ are determined so that the characteristic features near the minimum of the HFB (β_2, β_3) -PES, that is, the location of the minimum, and steepness in both the β_2 and β_3 deformations, are reproduced as closely as possible. A more detailed account of the steps (i) and (ii) of the mapping procedure is found in Ref. [10]. Constraining to the zero dipole moment $\beta_1 = 0$ in these steps is due to the fact that the energy surfaces are significantly soft against the β_1 deformation (see Sec. III A), and is in order to exploit the sd f-IBM parameters obtained from the previous study of Ref. [10].
- (iii) In the final step, the parameters $(\epsilon_p, \chi_{pf}, \chi_{pp}, \chi_{pd}, \kappa_1, \chi'_{df}, \chi'_{pd}, C_1)$ are determined so that the bosonic PESs in the (β_1, β_2) and (β_1, β_3) , with the β_3 and β_2 deformations being fixed at those values corresponding to the minimum in the (β_2, β_3) -deformation space, respectively, should be as similar as possible to the corresponding HFB PESs. Here it is assumed for simplicity that $\epsilon'_p = \epsilon'_f$ in Eq. (12), and that the strength of the dipole-dipole interaction equals that of the octupole-octupole one, i.e., $\kappa_1 = \kappa_3$. In addition, the fixed values of the parameters $\chi_{pf} = -0.5$, $\chi_{pd} = 0.2$, and $\chi'_{pd} = 0.5$ are used to reflect the fact that, as shown below, the PESs are not very sensitive to the β_1 deformation. Also their values are chosen to be smaller in magnitude than χ_{ff} , χ_{df} , and χ'_{df} parameters, assuming that couplings of p bosons to d and f bosons are weak. The remaining parameters $(\chi_{pp}, \chi'_{df}, C_1)$ are chosen to vary gradually as functions of boson number.

The mapped sd pf-IBM Hamiltonian is numerically diagonalized [46] in the space consisting of $n(= n_s + n_p + n_d + n_f)$ bosons, where n_s, n_p, n_d , and n_f are numbers

of s, p, d , and f bosons, respectively. As in the standard IBM, the total number of bosons n is conserved for each nucleus. Also the negative-parity p and f bosons are treated on the same footing as the positive-parity s and d bosons, that is, the numbers n_s, n_p, n_d , and n_f are all allowed to take values from 0 to n .

The $E2, E3$, and $E1$ transition probabilities are computed by using the corresponding transition operators

$$\hat{T}^{(E2)} = e_2 \hat{Q}, \quad \hat{T}^{(E3)} = e_3 \hat{O}, \quad \hat{T}^{(E1)} = e_1 \hat{D}', \quad (13)$$

where \hat{Q} and \hat{O} are the same quadrupole and octupole boson operators in Eq. (3) and Eq. (4), respectively, with the same values of the parameters χ as those used for the Hamiltonian. It was shown in Ref. [31] that the dipole transition operator should be expressed with parameters that exhibit some dependence on boson number, which is on the basis of the fact that the $E1$ transitions are accounted for to a large extent by the single-particle degrees of freedom or underlying shell structure. The $E1$ operator introduced in [31] is adopted here for \hat{D}' in (13) in the sd pf-boson model, and is given as

$$\begin{aligned} \hat{D}' = & s^\dagger \tilde{p} + p^\dagger \tilde{s} - \{1 - \alpha(n - 7)\} \\ & \times \left[(p^\dagger \times \tilde{d} + d^\dagger \times \tilde{p})^{(1)} - \beta (f^\dagger \times \tilde{d} + d^\dagger \times \tilde{f})^{(1)} \right], \end{aligned} \quad (14)$$

with the parameters $\alpha = 0.4$ and $\beta = 0.5$ [31]. For the sd f-boson model, \hat{D}' is simply given as

$$\hat{D}' = (d^\dagger \times \tilde{f} + f^\dagger \times \tilde{d})^{(1)}. \quad (15)$$

The boson effective charges e_2 and e_3 for the $E2$ and $E3$ operators are determined [10] for each nucleus so that the expectation values $\langle \hat{Q} \rangle$ and $\langle \hat{O} \rangle$ in the coherent state should be equal to the q_2^{\min} and q_3^{\min} moments obtained in the HFB that correspond to the minimum in the (β_2, β_3) -PES, that is,

$$e_2 = e_2^{(0)} q_2^{\min} (\langle \hat{Q} \rangle_{\min})^{-1} \quad (16)$$

$$e_3 = e_3^{(0)} q_3^{\min} (\langle \hat{O} \rangle_{\min})^{-1}. \quad (17)$$

Note that the multiplication by additional overall factors $e_2^{(0)} = 0.12 \text{ eb}$ and $e_3^{(0)} = 0.06 \text{ eb}^{3/2}$ in the above formulas is in order that the calculated $B(E2; 2_1^+ \rightarrow 0_1^+)$ and $B(E3; 3_1^- \rightarrow 0_1^+)$ should be of the same order of magnitudes as the experimental values. In addition, common $E2$ and $E3$ effective charges, which are determined by (16) and (17), are used for the sd f- and sd pf-IBM. The $E1$ boson charge e_1 is fixed to be the value employed in Ref. [31], i.e., $e_1 = 0.0054 \text{ eb}^{1/2}$, in the sd pf-boson model, while the constant value $e_1 = 0.008 \text{ eb}$ is adopted in the sd f-boson model. Also for the sd pf-model, in order to see if the parametrization of the operator in (14) is adequate the $E1$ transitions are computed by using \hat{D}' that is equal to \hat{D} (5) in the Hamiltonian with the constant effective charge $e_1 = 0.008 \text{ eb}^{1/2}$ as in the sd f-IBM.

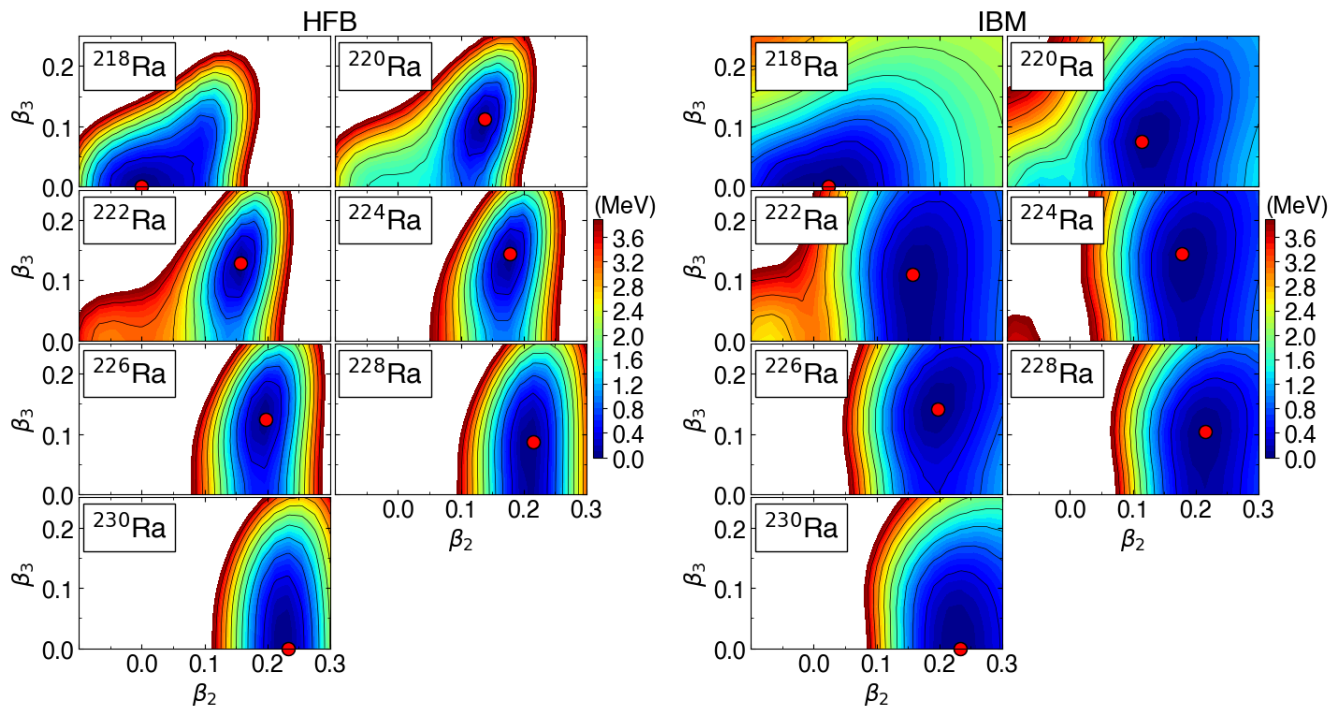


FIG. 1. Potential energy surfaces for $^{218-230}\text{Ra}$ in terms of the axial quadrupole β_2 and octupole β_3 deformations obtained from the HFB method using the Gogny-D1M EDF with the dipole deformation set to $\beta_1 = 0$, and the corresponding energy surfaces in the *spdf*-IBM. The minimum is indicated by the solid circle, and energy difference between neighboring contours is 0.4 MeV.

III. RESULTS

A. Potential energy surfaces

Figures 1, 2, and 3 show the two-dimensional PESs in the intrinsic (β_2, β_3) , (β_1, β_2) , and (β_1, β_3) deformations, respectively, computed for the $^{218-230}\text{Ra}$ isotopes using the constrained HFB method, and the corresponding mapped IBM PESs. The results for the Th isotopes are very similar to those for the Ra isotopes, and are therefore not shown. Note also that the (β_2, β_3) -PESs in Fig. 1 are also shown in Fig. 1 of Ref. [10].

The HFB (β_2, β_3) -PESs exhibit a pronounced octupole minimum for those Ra and Th nuclei with $N = 134$ or 136. For ^{226}Ra and ^{228}Ra , shown in Fig. 1, the potential is steep along the β_2 deformation, and is substantially soft in β_3 deformation. The behavior of the HFB PES for the Ra and Th nuclei with increasing neutron number points to a shape phase transition from nearly spherical to stable octupole deformed, and to octupole-soft intrinsic shapes [10, 16, 17]. The mapped IBM PESs follow the nucleon-number dependence and overall topology of the HFB PESs. The bosonic PESs are generally softer than the fermionic ones for those configurations corresponding to large deformations that are far from the minimum. This is a common feature of the mapping procedure, and is explained by the fact that the boson model space is

rather limited in comparison with the SCMF model. In the mean-field configurations at large deformations single(quasi)particle excitations become important, which are not included in the usual IBM space. The mapping is considered valid, as long as it is carried out specifically in the vicinity of the global minimum of the HFB PES, since the configurations near the global minimum are most relevant to the low-energy collective states. More detailed accounts of the mapping procedure are found in Refs. [10, 16, 17, 43].

The (β_1, β_2) -PESs obtained from the HFB calculation are in general steep in β_2 deformation, but are considerably soft along the β_1 deformation. Their global features also do not depend significantly on nucleon numbers, except for that of the nearly spherical nucleus ^{218}Ra . These observations indicate that the intrinsic shape of the Ra and Th nuclei is not sensitive to the dipole deformation. The HFB calculation also suggests that, for many of the Ra nuclei, a very shallow minimum occurs at finite β_1 deformation, as seen in Fig. 2. The corresponding IBM PESs exhibit similar systematic behaviors as the HFB PESs. The IBM PESs are constructed so as to reproduce mainly the location of the $\beta_1 \neq 0$ minimum, and the softness in the β_1 deformation.

The HFB PESs in the (β_1, β_3) plane, shown in Fig. 3, are β_1 soft, and more or less resemble a flat-bottomed potential in β_3 deformation particularly for ^{228}Ra and

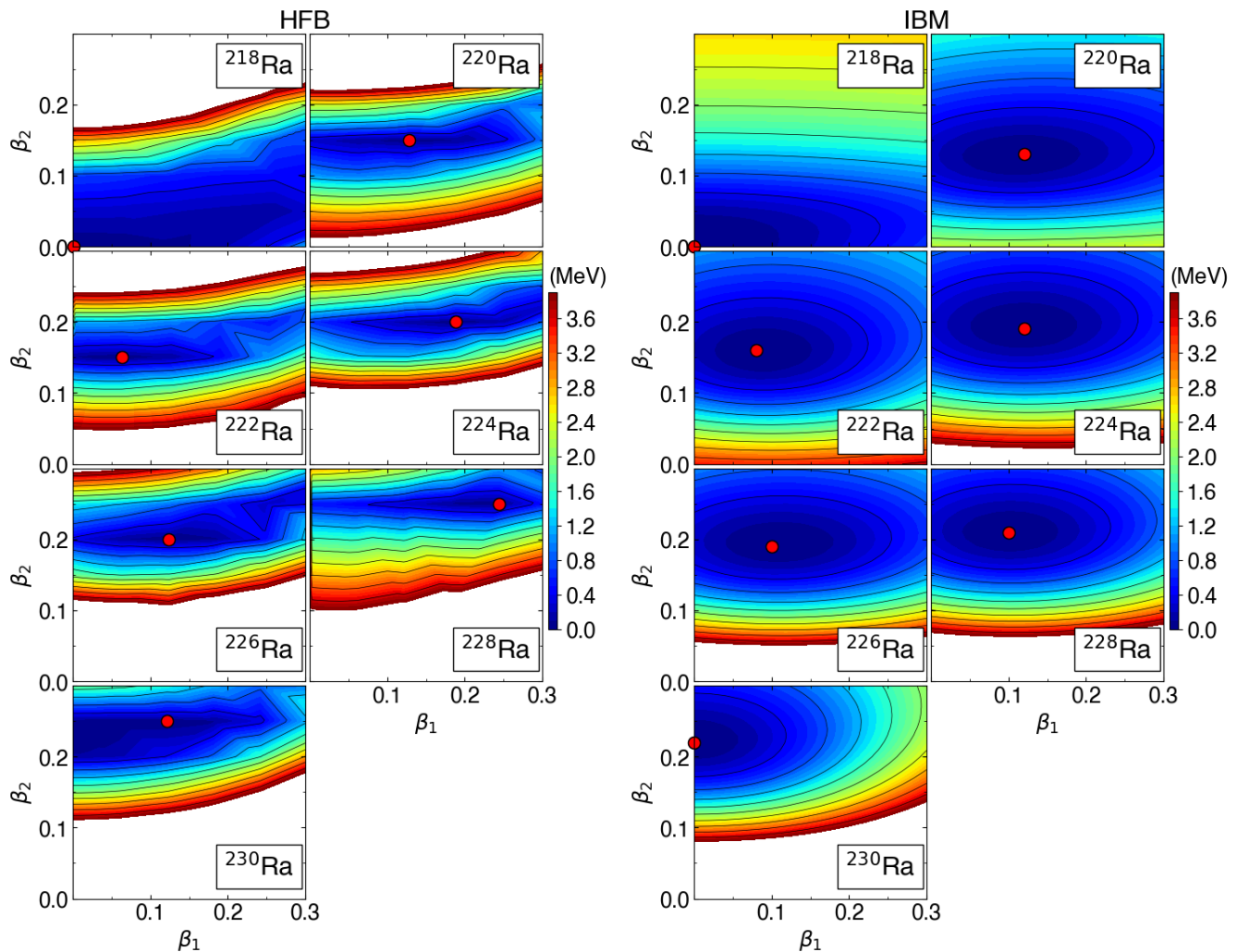


FIG. 2. Same as the caption to Fig. 1, but for the dipole β_1 and quadrupole β_2 deformations with the octupole deformation β_3 fixed to be the value corresponding to the minimum in the (β_2, β_3) space with $\beta_1 = 0$.

^{230}Ra . A shallow β_1 minimum is observed in the HFB PESs for ^{220}Ra , ^{222}Ra , ^{224}Ra , and ^{226}Ra . The IBM mapping is carried out so that the softness in β_1 and β_3 deformations, as well as the location of the minimum, of the HFB PES is reproduced as much as possible.

Some deviations in topology from the original HFB PESs are observed in the (β_1, β_2) and (β_1, β_3) planes. For instance, for ^{228}Ra and ^{230}Ra the mapped IBM (β_1, β_3) -PESs exhibits a $\beta_3 \neq 0$ minimum, while in the HFB PESs the minimum occurs on the $\beta_3 = 0$ axis. The deviations can be accounted for by the limited analytical form of the *spdf*-IBM, which does not have degrees of freedom sufficient to reproduce accurately the HFB PESs. In addition, the *spdf*-IBM parameters relevant to the dipole deformations are chosen to reproduce the global features of both the HFB (β_1, β_2) - and (β_1, β_3) -PESs, and it is not very obvious to reproduce all the details of the two surfaces simultaneously.

To see possible effects of the p boson degree of freedom on the energy surface, Fig. 4 depicts the *spdf*-IBM (β_2, β_3) -PESs for ^{222}Ra , with the β_1 deformation being fixed at several different values. ^{222}Ra is taken here as an illustrative case, since as shown below the inclusion of p bosons has pronounced influences on energy spectra in this nucleus. One can see from Fig. 4 that, with the increasing β_1 deformation, the (β_2, β_3) -PES becomes steeper in β_3 , and the minimum occurs at larger β_2 and β_3 deformations. For a relatively small dipole deformation of $\beta_1 = 0.05$, near which the equilibrium minimum is found in the (β_1, β_2) - and (β_1, β_3) -PESs, p bosons do not appear to have significant effects of altering the topology of the (β_2, β_3) -PES.

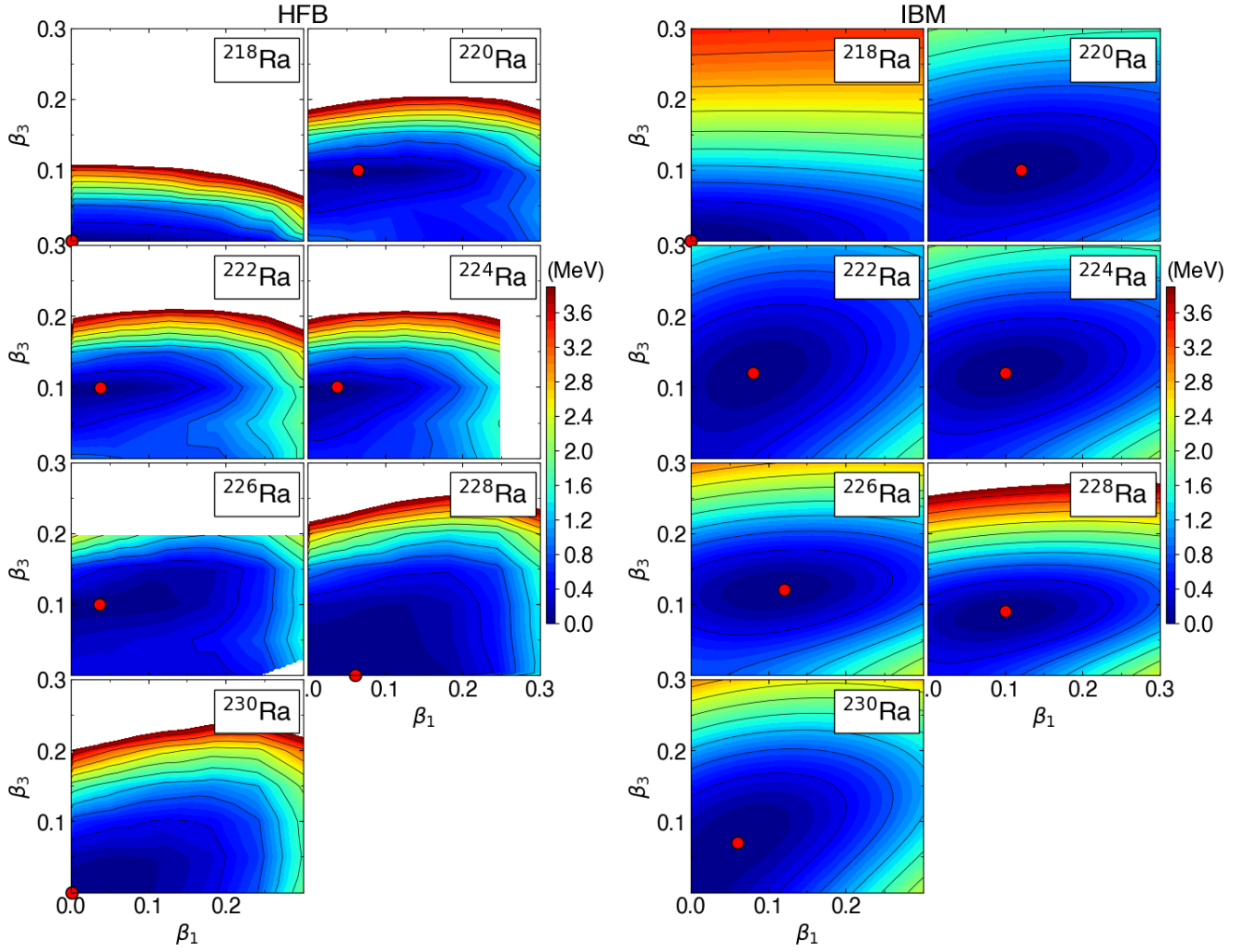


FIG. 3. Same as the caption to Fig. 1, but for the dipole β_1 and octupole β_3 deformations with the quadrupole deformation β_2 fixed to be the value corresponding to the minimum in the (β_2, β_3) space with $\beta_1 = 0$.

B. IBM parameters

The *spdf*-IBM parameters employed in the present work are given in Table I. The parameters (ϵ_d , κ_2 , χ_{dd} , C_2 , ϵ_f , χ_{ff} , κ_3 , χ_{df} , C_3) for the *sdf*-IBM Hamiltonian are also found in Fig. 3 of Ref. [10]. The *d*-boson energy basically decreases with N , as the quadrupole collectivity enhances. As in the previous mapped *sdf*-IBM calculations the single-*f* boson energy ϵ_f exhibits a parabolic behavior, reaching a minimum in magnitude near $N = 136$ (Ra) and $N = 134$ (Th), in which the (β_2, β_3) -PES exhibits a pronounced octupole deformation. What is of particular interest is the fact that the *p*-boson energy ϵ_p is here systematically lower in magnitude than the *f*-boson one, and is of the same order of magnitude as or even lower than the *d*-boson energy for many of the nuclei considered. This is because the (β_1, β_2) and (β_1, β_3) energy surfaces are in many cases soft in β_1 deformation,

and the mapping procedure incorporates such features in the parameters (see Figs. 2 and 3). The κ_2 and $\kappa_3 (= \kappa_1)$ parameters are almost constant but shows a gradual decreases in magnitude with neutron number. The derived parameter χ_{dd} is close to the SU(3) value $-\sqrt{7}/2$ for most of the nuclei with $N \geq 134$, which exhibit a strong prolate deformation.

The χ_{pp} parameter exhibits a substantial variation from $N = 132 - 136$. For $N = 130$ and 132 , the chosen χ_{pp} values are of the same order of magnitude as χ_{ff} , indicating that the dipole correlations can be as pronounced as the octupole correlations in these transitional nuclei. For the nuclei with $N = 130$ and 132 , the large χ_{pp} values are required to produce the β_1 softness of the (β_1, β_2) - and (β_1, β_3) -PESs with limited boson numbers. Both χ_{ff} and χ_{df} parameters concern the degree of octupole deformation, and becomes maximal for those nuclei near $N = 134$ or 136 , for which the octupole mini-

TABLE I. Parameters for the *spdf*-IBM Hamiltonian adopted in the present work for the nuclei $^{218-230}\text{Ra}$ and $^{220-232}\text{Th}$. ϵ_d , ϵ_f , ϵ_p , κ_2 , κ' , κ_3 are in keV units. Fixed values $\chi_{pf} = -0.5$, $\chi_{pd} = 0.2$, and $\chi'_{pd} = 0.5$ are used, and the dipole-dipole interaction strength is assumed to be equal to the octupole-octupole one, $\kappa_1 = \kappa_3$.

	ϵ_d	ϵ_f	ϵ_p	κ_2	χ_{dd}	χ_{pp}	χ_{ff}	κ'	κ_3	χ_{df}	χ'_{df}	C_2	C_3	C_1
^{218}Ra	363	-672	-701	-40	-0.50	1.50	1.20	0	-26	-1.20	0.60	10.0	7.0	1.8
^{220}Ra	533	-789	-505	-53	-1.30	1.50	1.70	-15	-26	-2.20	1.10	7.6	7.0	3.2
^{222}Ra	213	-526	-241	-52	-1.30	0.90	1.90	-11	-22	-1.90	0.95	7.2	5.6	3.1
^{224}Ra	266	-476	-130	-52	-1.30	0.50	1.80	-14	-20	-2.10	1.10	6.5	6.8	2.5
^{226}Ra	318	-755	-414	-46	-1.30	0.50	1.80	-11	-19	-2.60	1.10	6.3	6.9	2.0
^{228}Ra	264	-800	-512	-44	-1.30	0.50	1.80	-10	-19	-2.20	1.10	5.8	8.0	2.0
^{230}Ra	207	-738	-530	-41	-1.30	0.50	1.60	-8	-18	-1.80	0.90	5.5	4.9	2.0
^{220}Th	619	-899	-940	-49	-0.30	1.50	1.20	0	-27	-1.20	0.60	7.3	4.0	2.0
^{222}Th	475	-960	-657	-53	-1.10	1.50	1.90	-17	-27	-1.90	0.95	6.7	6.2	2.8
^{224}Th	276	-398	-151	-50	-1.34	0.90	1.68	-11	-24	-1.75	0.88	6.8	7.0	2.7
^{226}Th	356	-600	-254	-53	-1.32	0.70	1.80	-15	-22	-2.00	1.00	6.1	5.5	2.2
^{228}Th	482	-739	-364	-51	-1.32	0.50	1.82	-16	-16	-2.40	1.20	5.6	5.0	2.0
^{230}Th	418	-683	-362	-49	-1.32	0.50	1.80	-15	-16	-1.90	0.95	5.3	5.1	1.8
^{232}Th	373	-657	-400	-47	-1.30	0.50	1.70	-13	-16	-1.50	0.75	5.1	4.4	2.0

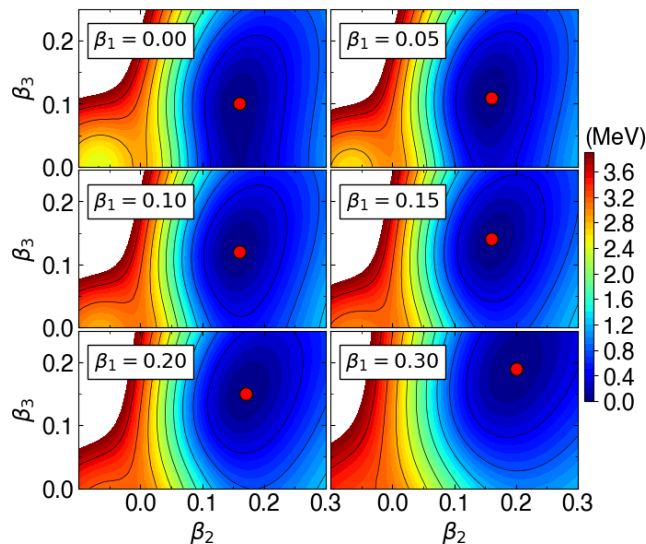


FIG. 4. Mapped *spdf*-IBM (β_2, β_3) -PESs for ^{222}Ra with the β_1 deformation being fixed at several different values.

mum is most pronounced. The values of the χ'_{df} parameter are chosen to be $\chi'_{df} \approx \chi_{df}/2$, for simplicity. Also the absolute values $|\chi_{df}|$ and $|\chi'_{df}|$ are generally larger than $|\chi_{pd}| = 0.2$ and $|\chi'_{pd}| = 0.5$, respectively, assuming that the coupling of p to d bosons is weaker than that of f to d bosons.

The scale factor C_2 for the β_2 deformation only exhibits a gradual decrease with neutron number. The factor C_3 used in Ref. [10] is here slightly modified so that the minima in all the (β_2, β_3) , (β_1, β_2) and (β_1, β_3) surfaces are consistently reproduced to a certain accuracy. This is the reason why this coefficient exhibits a

rather irregular behavior with neutron number. The C_1 coefficient here displays a characteristic feature of being maximal near $N = 132$, in which the energy surface is particularly soft in the (β_1, β_2) and (β_1, β_3) deformation spaces.

C. Low-energy spectra

Figures 5 and 6 display, respectively, the predicted energy spectra for the positive-parity yrast states in the ground-state $K = 0^+$ band, and for the negative-parity yrast states in the $K = 0^-$ band in the mapped *sdf*-IBM and *spdf*-IBM in comparison with the experimental data [47].

The *sdf*- and *spdf*-boson model calculations both suggest that the positive-parity energy levels gradually decrease as functions of the neutron number, reflecting the enhancement of the quadrupole collectivity or shape phase transitions from the nearly spherical to strongly prolate deformed regimes. The two boson models appear to give rise to qualitatively very similar results. However, the *spdf*-boson model gives the positive-parity levels that are rather higher in energy than those in the *sdf*-IBM. These differences are inferred from the structure of the calculated wave functions of the relevant states, as shown in Fig. 7. For the nuclei $^{222-228}\text{Ra}$ [Figs. 7(c)-7(d)], the expectation values of the f -boson number operator $\langle \hat{n}_f \rangle$ in the wave functions for the even-spin states in the ground-state $K = 0^+$ band in the *spdf*-IBM are systematically larger than those in the *sdf*-IBM. These effects, together with the presence of p bosons, could account for the quantitative differences between the *sdf*-IBM and *spdf*-IBM results for the positive-parity states.

As shown in Fig. 6, both the *sdf*-IBM and *spdf*-IBM reproduce the observed parabolic behaviors of the negative-

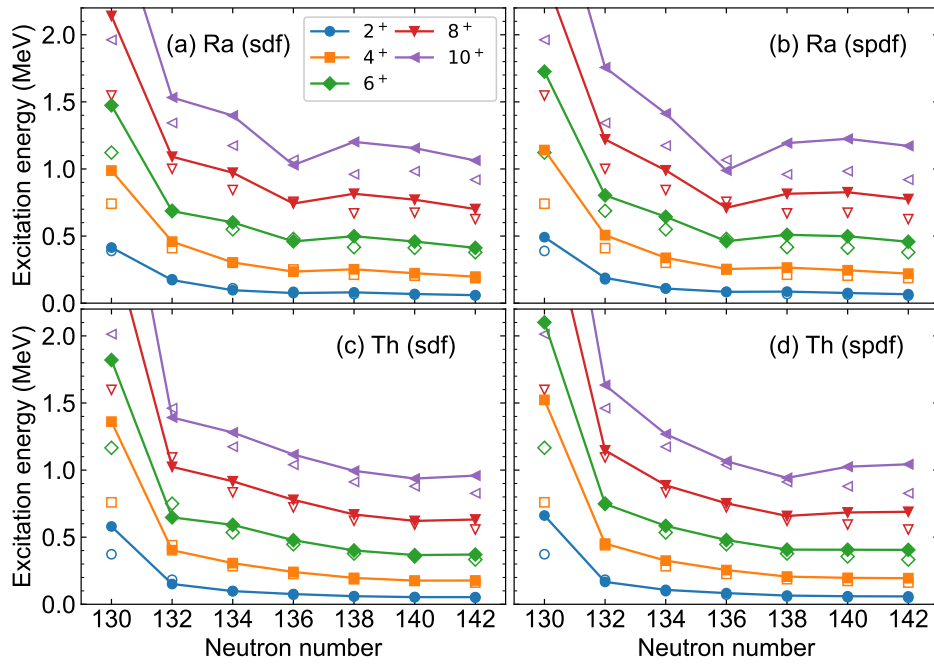


FIG. 5. Calculated excitation energies for even-spin positive-parity yrast states for $^{218-230}\text{Ra}$ and $^{220-232}\text{Th}$ within the mapped *sdf*-IBM and *spdf*-IBM (solid symbols connected by lines). The corresponding experimental values, represented by open symbols, are taken from NNDC [47].

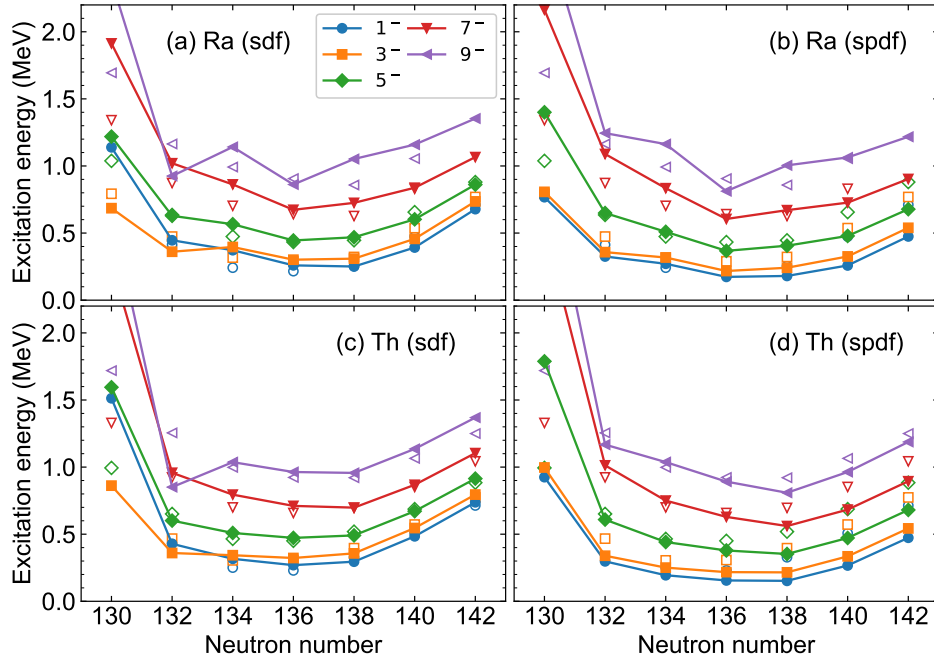


FIG. 6. Same as the caption to Fig. 5, but for the odd-spin negative-parity yrast states.

parity energy spectra in $^{218-230}\text{Ra}$ and $^{220-232}\text{Th}$ as functions of the neutron number, with the bandhead 1^- state of the possible $K = 0^-$ band being lowest in energy near

$N = 136$. The effects of including p bosons are such that the 1^- bandhead of the $K = 0^-$ bands are systematically lowered. For those Ra and Th nuclei with $N \leq 132$,

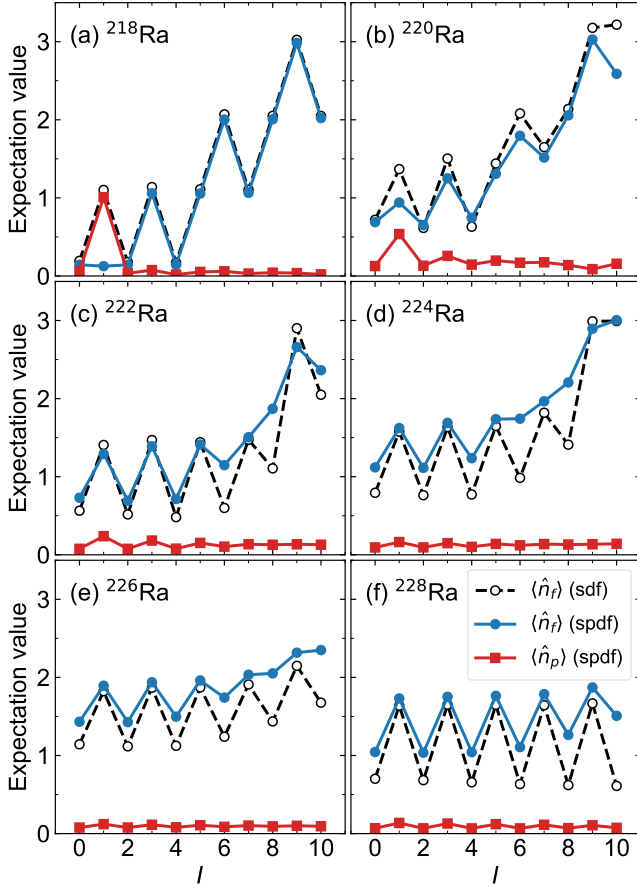


FIG. 7. Expectation values of the f -boson number operator $\langle \hat{n}_f \rangle$ in the sdf -IBM and $spdf$ -IBM, and of the p -boson number operator $\langle \hat{n}_p \rangle$ in the $spdf$ -IBM for the even-spin positive-parity and odd-spin negative-parity yrast states with increasing spin I in $^{218-228}\text{Ra}$.

in the sdf -IBM the lowest-energy negative-parity state is the 3^- state, and the 1^- level is above that of the 3^- one. Also the 9^- level appears below the 7^- level for ^{220}Ra and ^{222}Th in the sdf -IBM. In the $spdf$ -IBM results, however, the 1^- state is predicted to be the lowest-lying negative-parity state for these nuclei, which is consistent with the experimental data for ^{220}Ra in particular. The irregularity in the order of the 7^- and 9^- at $N = 132$ appears to be removed in the $spdf$ -IBM. Overall the $spdf$ -IBM underestimates the observed 1^- level. This is, to a large extent, due to the fact that in the present IBM mapping calculation the single p -boson energy is substantially low with respect to those of d and f bosons (cf. Table I).

It is seen from Fig. 7 that the contributions of f bosons to the wave functions for the odd-spin negative-parity states in the $spdf$ -IBM are within the range $\langle \hat{n}_f \rangle \approx 1.5 - 3.0$ particularly for $^{222-228}\text{Ra}$, which are of the same order of magnitude as those in the sdf -IBM. The contributions of p bosons are mostly minor for these nuclei, and are rather constant with the increasing spin. These

results suggest that the odd-spin negative-parity yrast states in deformed Th and Ra nuclei are mostly made of f bosons even in the presence of p bosons. Only for the ^{218}Ra nucleus (also for ^{220}Th), the 1^- wave function is characterized by the one- p -boson configurations, $\langle \hat{n}_p \rangle \approx 1$, while the f -boson content is minor.

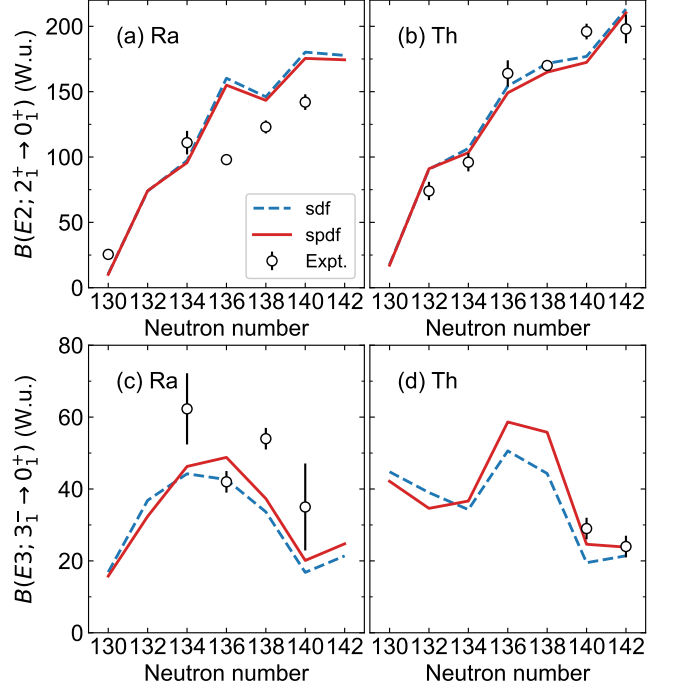


FIG. 8. Calculated $B(E2)$ and $B(E3)$ values in Weisskopf units (W.u.) for $^{218-230}\text{Ra}$ and $^{220-232}\text{Th}$ in the sdf -IBM and $spdf$ -IBM, and the corresponding experimental data [5, 47–49].

D. Transition properties

Figure 8 exhibits the $B(E2; 2_1^+ \rightarrow 0_1^+)$ and $B(E3; 3_1^- \rightarrow 0_1^+)$ values in Weisskopf units (W.u.) calculated by using the corresponding transition operators in (13) with the boson charges determined by the formulas of Eqs. (16) and (17). The $B(E2)$ values only increase with N as the quadrupole collectivity develops. The calculated $B(E2)$ values are of the same order of magnitudes as the experimental values [5, 47–49], except for ^{224}Ra ($N = 136$), for which the mapped IBM overestimates the data approximately by a factor of 1.5. In addition, the $B(E2)$ values obtained from the mapped $spdf$ -IBM do not differ quantitatively from those from the sdf -IBM. The calculated $B(E3; 3_1^- \rightarrow 0_1^+)$ values, given in Figs. 8(c) and 8(d), show an inverse parabola with the maximal value near $N = 134$ (Ra) and $N = 136$ (Th). This behavior of the $B(E3)$ values confirms that the octupole collectivity is most enhanced near $N = 136$, and

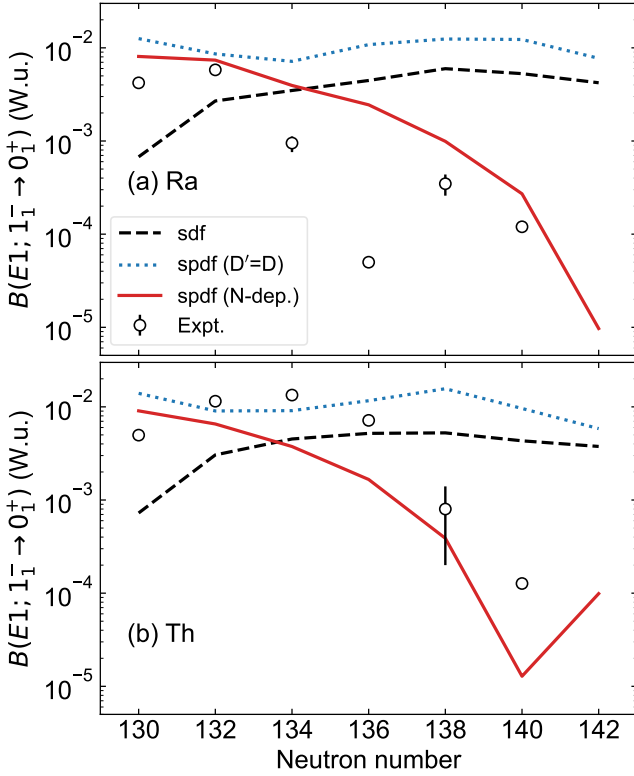


FIG. 9. Calculated $B(E1; 1_1^- \rightarrow 0_1^+)$ values in W.u. for $^{218-230}\text{Ra}$ and $^{220-232}\text{Th}$ within the mapped *sdf*-IBM and *spdf*-IBM. Two *spdf*-IBM results denoted $D' = D$ and N -dep. refer, respectively, to the calculations with the $E1$ operator defined by (14) and that defined as $\hat{D}' = \hat{D}$ with the constant effective charge $e_1 = 0.008 eb^{1/2}$. Experimental data are adopted from [5, 47–50]. Note that the experimental data for ^{224}Ra and ^{228}Ra shown in (a) are upper and lower limits, respectively.

correlates with the finding that the calculated negative-parity energy levels are lowest in energy near those neutron numbers. The $B(E3)$ values obtained from the mapped *spdf*-IBM are slightly smaller than those in the *sdf*-IBM for $N = 130$ and 132 , whereas in octupole deformed region with $N \geq 134$ more enhanced $E3$ transitions are suggested by the *spdf*-IBM.

Figure 9 depicts the predicted $B(E1; 1_1^- \rightarrow 0_1^+)$ values in W.u., for $^{218-230}\text{Ra}$ and $^{220-232}\text{Th}$. The *sdf*-IBM calculation with the $E1$ operator of the form of (15) indicates a slight increase from $N = 130 - 134$, but suggests only a gradual variation for $N \geq 136$, which contradicts the data. The $B(E1; 1_1^- \rightarrow 0_1^+)$ values in the *spdf*-IBM obtained by using the $E1$ operator in which for \hat{D}' the same dipole operator \hat{D} (5) as in the *spdf*-boson Hamiltonian (2) is used (denoted $D' = D$ in the figure) do not exhibit any significant variation with N . The $B(E1)$ values obtained from the *spdf*-IBM with the $E1$ operator defined in (14) (N -dep.) show an overall decrease by orders of magnitudes as functions of N , consistently with the ex-

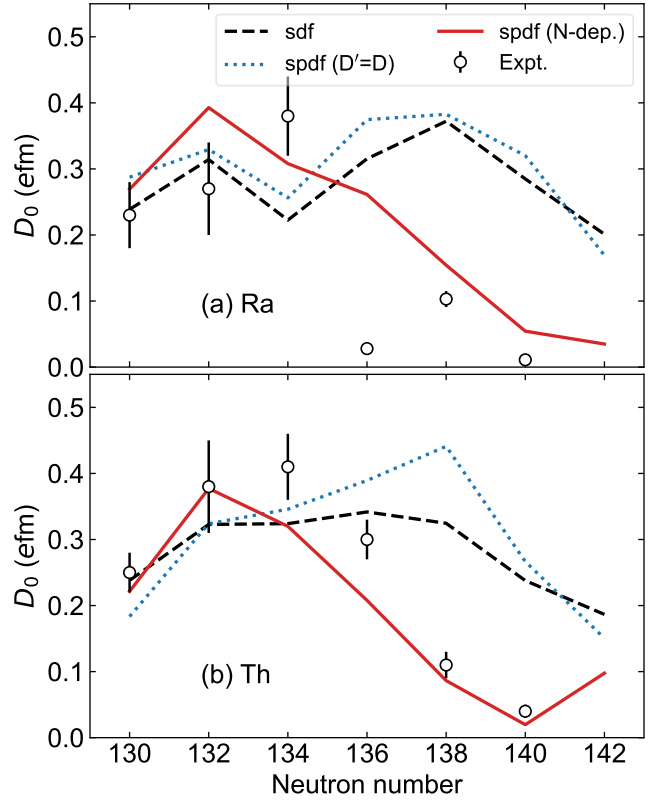


FIG. 10. Calculated $E1$ moment D_0 in efm for $^{218-230}\text{Ra}$ and $^{220-232}\text{Th}$ in the *sdf*-IBM, and in the *spdf*-IBM using the $E1$ operator with $\hat{D}' = \hat{D}$ and that which depends on the neutron number N defined in (14). Experimental data are taken from Ref. [51].

perimental systematic. A significant deviation from the experimental data in either choice of the $E1$ transition operator in the *spdf*-IBM is found for ^{224}Ra for which the present calculations provide the $B(E1; 1_1^- \rightarrow 0_1^+)$ value that is by orders of magnitude larger than the experimentally estimated upper limit [5].

Figure 10 shows the predicted intrinsic dipole moment of the studied Ra and Th nuclei within the *sdf*-IBM and *spdf*-IBM using the $E1$ operator with $\hat{D}' = \hat{D}$ and that which depends on the neutron number N (14). The experimental dipole moments [51] included in the figure were those obtained as averages of transition moments of some high-spin states with $I \geq 6$. As in Ref. [31], the D_0 moments are here obtained from the calculated $B(E1; 6_1^+ \rightarrow 5_1^-)$ transition rates, and using the formula

$$B(E1; I \rightarrow I') = \frac{3}{4\pi} D_0^2 (I1K0|I'K'), \quad (18)$$

where $(I1K0|I'K')$ denotes a Clebsch-Gordan coefficient, and the quantum numbers $K = K' = 0$ for the initial (I) and final (I') states, respectively. It is seen in the figure that the calculated D_0 moments in the *spdf*-IBM with the $E1$ operator of (14) exhibit systematic and ab-

solute values that are consistent with the experimental data, except for the ^{224}Ra nucleus. The calculation in the *sdf*-IBM, and the one in the *spdf*-IBM with the $E1$ operator corresponding to the same dipole operator as in the Hamiltonian do not appear to be able to reproduce the correct observed behaviors of this quantity for deformed region, $N \geq 138$.

E. Detailed energy spectra

Figure 11 displays the calculated low-energy spectra of both parities for the isotopes ^{222}Ra , ^{224}Ra , ^{228}Ra , and ^{228}Th within the mapped *sdf*-IBM and *spdf*-IBM. These nuclei are here chosen with a renewed interest from an experimental point of view, since updated data have recently been provided [5, 47–49]. Comparisons of the theoretical and experimental $E2$, $E3$, and $E1$ transition properties for these nuclei are given in Tables II–VII.

TABLE II. $B(E\lambda)$ transition strengths in W.u. for ^{222}Ra calculated within the *sdf*-IBM and *spdf*-IBM. The corresponding experimental data are taken from NNDC [47].

$B(E\lambda; I_i^\pi \rightarrow I_f^\pi)$	<i>sdf</i> -IBM	<i>spdf</i> -IBM	Expt.
$B(E2; 2_1^+ \rightarrow 0_1^+)$	97	96	$112.8_{-8.2}^{+9.6}$
$B(E2; 4_1^+ \rightarrow 2_1^+)$	134	131	123 ± 14
$B(E2; 6_1^+ \rightarrow 4_1^+)$	134	121	135_{-21}^{+24}
$B(E2; 8_1^+ \rightarrow 6_1^+)$	112	99	119_{-28}^{+36}
$B(E2; 10_1^+ \rightarrow 8_1^+)$	82	92	139_{-48}^{+76}
$B(E2; 3_1^- \rightarrow 1_1^-)$	96	103	98_{-40}^{+49}
$B(E2; 5_1^- \rightarrow 3_1^-)$	116	122	109_{-26}^{+30}
$B(E2; 7_1^- \rightarrow 5_1^-)$	117	121	95_{-38}^{+74}
$B(E2; 9_1^- \rightarrow 7_1^-)$	45	65	$2.7_{-0.7}^{+1.0} \times 10^2$
$B(E1; 1_1^- \rightarrow 0_1^+)$	3.5×10^{-3}	3.9×10^{-3}	$9.5_{-1.7}^{+1.9} \times 10^{-4}$
$B(E1; 1_1^- \rightarrow 2_1^+)$	3.3×10^{-3}	6.3×10^{-3}	$1.86_{-0.34}^{+0.40} \times 10^{-3}$
$B(E1; 3_1^- \rightarrow 2_1^+)$	4.9×10^{-3}	4.6×10^{-3}	$4.1_{-1.4}^{+1.7} \times 10^{-3}$
$B(E1; 5_1^- \rightarrow 4_1^+)$	5.6×10^{-3}	4.5×10^{-3}	$1.23_{-0.24}^{+0.60} \times 10^{-3}$
$B(E1; 6_1^+ \rightarrow 5_1^-)$	2.3×10^{-3}	4.4×10^{-3}	$2.11_{-0.40}^{+0.44} \times 10^{-3}$
$B(E1; 7_1^- \rightarrow 6_1^+)$	6.5×10^{-3}	4.8×10^{-3}	$2.4_{-2.1}^{+1.2} \times 10^{-3}$
$B(E1; 8_1^+ \rightarrow 7_1^-)$	4.8×10^{-3}	5.2×10^{-3}	$2.65_{-0.66}^{+0.75} \times 10^{-3}$
$B(E1; 9_1^- \rightarrow 8_1^+)$	6.3×10^{-3}	4.9×10^{-3}	$4.9_{-1.4}^{+1.8} \times 10^{-3}$
$B(E1; 10_1^+ \rightarrow 9_1^-)$	4.5×10^{-3}	4.3×10^{-3}	$3.2_{-1.1}^{+1.6} \times 10^{-3}$

In Fig. 11 the calculated ground-state band in both the *sdf*- and *spdf*-boson models for ^{222}Ra is rather stretched in comparison with experiment. As mentioned above, the $K = 0^-$ band in the *sdf*-IBM exhibits inversions of levels 1^- and 3^- , and 7^- and 9^- . The wrong order of levels is lifted in the *spdf*-IBM energy spectra. Neither of the two mapped boson models, however, produces the $K = 0^-$ band with moment of inertia consistent with that of the observed $K = 0^-$ band. The irregularity in the predicted $K = 0^-$ bands could be attributed to the fact that significant amounts of f -boson configurations enter the wave functions of high-spin states with spin $I \geq 7$ [see Fig. 7(c)]. The predicted ground-state bands in *sdf*

and *spdf* frameworks also exhibit some irregularity, i.e., the 6^+ energy level is rather close to the 4^+ level. The f -boson contributions appear to play a role also in these positive-parity states. The IBM mapping calculations yield the non-yrast 0_2^+ and 2_2^+ levels with energies consistent with the experimental values [47]. From Fig. 11 one can see that the mapped *spdf*-IBM provides an improved description of these levels over the *sdf*-IBM. In the *sdf*-IBM, for both the 0_2^+ and 2_2^+ states the expectation value $\langle \hat{n}_f \rangle \approx 2$, indicating the double-octupole phonon nature as suggested in the earlier mapped *sdf*-IBM calculation based on the relativistic EDF [17] and in some experimental studies, e.g., Ref. [52]. The *spdf*-IBM wave functions of these states are characterized by dominant f -boson contributions with the expectation value $\langle \hat{n}_f \rangle \approx 1.3$ and the p -boson contributions with $\langle \hat{n}_p \rangle \approx 0.6$.

As shown in Table II, by the inclusion of p bosons $B(E2)$ values for the in-band transitions in the ground-state band for ^{222}Ra are generally reduced, while those in the negative-parity band are enhanced. The $B(E1)$ rates are, in general, of the same order of magnitude as the experimental values [47]. In Table III the calculated $E2$ and $E3$ reduced matrix elements are compared with the recent experimental data [48]. Up to sign most of the predicted matrix elements are consistent with the data. The *spdf*-IBM results for the $E3$ matrix elements are overall larger in magnitude than those in the *sdf*-IBM.

The nucleus ^{224}Ra was experimentally revealed to be empirical evidence for the permanent octupole deformation [5]. The (β_2, β_3) -PES of this nucleus exhibits a distinct minimum with $\beta_3 \neq 0$, and an approximate alternating parity band is suggested experimentally. It is seen from Fig. 11 that the mapped IBM calculations in both the *sdf* and *spdf* versions yield low-energy spectra of states with both parities that are consistent with the

TABLE III. Calculated and experimental [48] reduced $E2$ and $E3$ matrix elements in $eb^{\lambda/2}$ units for ^{222}Ra .

$\langle I E\lambda I' \rangle$	<i>sdf</i> -IBM	<i>spdf</i> -IBM	Expt.
$\langle 2_1^+ E2 2_1^+ \rangle$	-2.4	-2.3	-1.3 ± 0.5
$\langle 4_1^+ E2 2_1^+ \rangle$	-3.1	-3.1	2.98 ± 0.15
$\langle 6_1^+ E2 4_1^+ \rangle$	3.7	3.5	3.57 ± 0.18
$\langle 8_1^+ E2 6_1^+ \rangle$	3.9	3.7	4.15 ± 0.23
$\langle 3_1^- E2 1_1^- \rangle$	-2.3	2.4	2.35 ± 0.22
$\langle 5_1^- E2 3_1^- \rangle$	3.2	-3.3	3.1 ± 0.4
$\langle 7_1^- E2 5_1^- \rangle$	-3.7	-3.8	4.4 ± 0.4
$\langle 9_1^- E2 7_1^- \rangle$	-2.6	3.1	6.0 ± 1.0
$\langle 1_1^- E3 2_1^+ \rangle$	0.9	-1.0	0.85 ± 0.24
$\langle 3_1^- E3 0_1^+ \rangle$	-1.0	-1.0	1.13 ± 0.09
$\langle 3_1^- E3 2_1^+ \rangle$	1.0	1.1	-0.9 ± 0.5
$\langle 3_1^- E3 4_1^+ \rangle$	0.9	1.0	$2.6_{-0.9}^{+0.6}$
$\langle 4_1^+ E3 1_1^- \rangle$	-0.8	0.9	-2.1 ± 0.5
$\langle 5_1^- E3 2_1^+ \rangle$	-1.4	1.4	1.79 ± 0.20
$\langle 5_1^- E3 4_1^+ \rangle$	-1.2	1.3	-1.7 ± 1.0
$\langle 7_1^- E3 4_1^+ \rangle$	-1.6	1.7	$3.3_{-0.5}^{+0.3}$

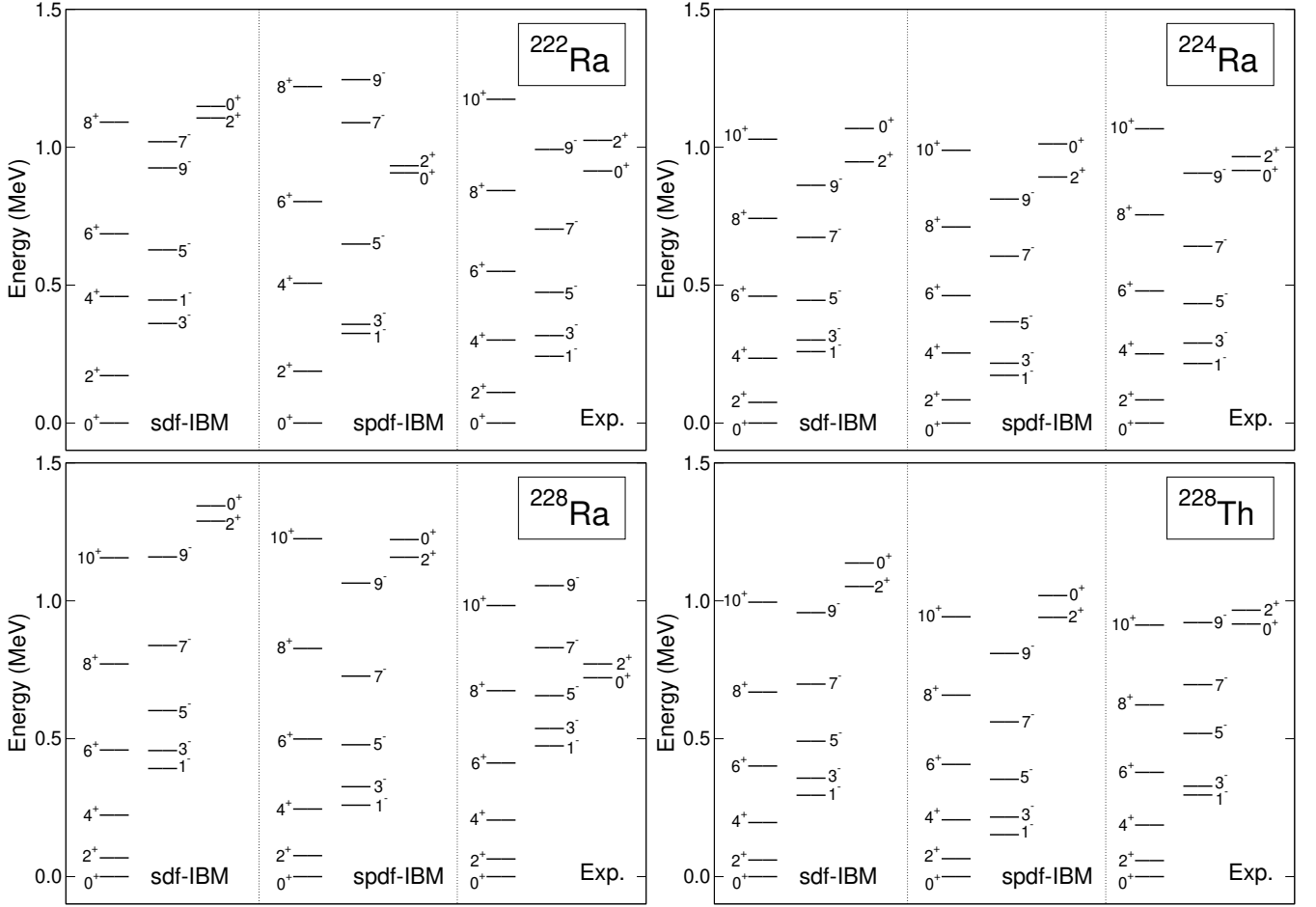


FIG. 11. Low-energy spectra for ^{222}Ra , ^{224}Ra , ^{228}Ra , and ^{228}Th calculated with the mapped *sdf*-IBM and *spdf*-IBM, and the corresponding experimental data [5, 47, 49].

experimental data. An improvement over the *sdf*-IBM could be that the 1^- bandhead of the $K = 0^-$ band in the *spdf*-IBM is found below the 4^+ level, which is indeed observed experimentally. The non-yrast 0_2^+ and 2_2^+ levels are lowered in energy in the *spdf*-IBM, but the order of these levels is at variance with experiment. However, the calculated 2_2^+ state may here be of different character, e.g., bandhead of the γ -vibrational band, from the 0_2^+ state, and probably should not be considered a member of the band built on the 0_2^+ state. Both of these states are of double-octupole phonon nature in the present *sdf*-IBM, while *f* and *p* boson configurations make appreciable contributions to the wave functions in the *spdf*-IBM, since the expectation values $\langle \hat{n}_f \rangle \approx 1.5$ and $\langle \hat{n}_p \rangle \approx 0.3$. As shown in Table IV, the calculated $B(E2)$ values generally overestimate the experimental values, while the $B(E3)$ values obtained in either of the two boson models are more or less within error bars of the experimental data. As is well known, the $B(E1)$ transition rates for ^{224}Ra are anomalously small as compared with the neighboring isotopes ^{222}Ra and ^{226}Ra [see also Fig. 9(a)]. The present IBM mapping calculations, even that which in-

cludes the *p*-boson degrees of freedom, fail to reproduce this observed systematic.

The (β_2, β_3) -PES of the ^{228}Ra nucleus is shown to be particularly soft along the β_3 deformation. The observed energy spectra show features that the $K = 0^-$ yrast band decouples from the ground-state $K = 0^+$ band, forming separate rotational bands [47]. This feature is reproduced in the *sdf*-IBM, since as shown in Fig. 11 the 1^- bandhead of the $K = 0^-$ band appears close to the 6^+ level. The calculated $K = 0^-$ band in the *spdf*-IBM is, however, much lower than the experimental counterpart. This suggests that the contributions of the negative-parity bosons to the low-lying $K = 0^-$ band for ^{228}Ra are rather overestimated in the *spdf*-IBM. The 0_2^+ and 2_2^+ states in the *spdf*-IBM are lower in energy than those in the *sdf*-IBM, but are considerably higher than the experimental values. These non-yrast states are predicted to be formed by the coupling of approximately two *f* bosons in the *sdf* model, and are in the *spdf* model comprised of large fractions of the *f*-boson ($\langle \hat{n}_f \rangle \approx 1.7$) and minor contributions from the *p*-boson components ($\langle \hat{n}_p \rangle \approx 0.2$).

In Table V the mapped *spdf*-IBM gives smaller $B(E2)$ values than the *sdf*-IBM for ^{228}Ra . The calculated

TABLE IV. Same as the caption to Table II, but for ^{224}Ra . Experimental data are from Refs. [5, 47].

$B(E\lambda; I_i^\pi \rightarrow I_f^\pi)$	<i>sdf</i> -IBM	<i>spdf</i> -IBM	Expt.
$B(E2; 2_1^+ \rightarrow 0_1^+)$	160	155	98 ± 3
$B(E2; 2_2^+ \rightarrow 0_1^+)$	0.8	1.2	1.3 ± 0.5
$B(E2; 4_1^+ \rightarrow 2_1^+)$	221	210	137 ± 5
$B(E2; 6_1^+ \rightarrow 4_1^+)$	222	195	156 ± 12
$B(E2; 8_1^+ \rightarrow 6_1^+)$	201	184	180 ± 60
$B(E2; 3_1^- \rightarrow 1_1^-)$	168	173	93 ± 9
$B(E2; 5_1^- \rightarrow 3_1^-)$	199	204	190 ± 60
$B(E3; 1_1^- \rightarrow 2_1^+)$	106	128	210 ± 40
$B(E3; 3_1^- \rightarrow 0_1^+)$	43	49	42 ± 3
$B(E3; 3_1^- \rightarrow 2_1^+)$	52	62	< 600
$B(E3; 5_1^- \rightarrow 2_1^+)$	61	70	61 ± 17
$B(E1; 1_1^- \rightarrow 0_1^+)$	4.5×10^{-3}	2.4×10^{-3}	$< 5 \times 10^{-5}$
$B(E1; 1_1^- \rightarrow 2_1^+)$	5.8×10^{-3}	4.0×10^{-3}	$< 1.3 \times 10^{-4}$
$B(E1; 3_1^- \rightarrow 2_1^+)$	6.4×10^{-3}	3.1×10^{-3}	$3.9_{-1.4}^{+1.7} \times 10^{-5}$
$B(E1; 5_1^- \rightarrow 4_1^+)$	7.3×10^{-3}	3.2×10^{-3}	$4_{-2}^{+3} \times 10^{-5}$
$B(E1; 7_1^- \rightarrow 6_1^+)$	8.4×10^{-3}	3.3×10^{-3}	$< 3 \times 10^{-4}$

TABLE V. Same as the caption to Table II, but for ^{228}Ra . Experimental data are from Ref. [47].

$B(E\lambda; I_i^\pi \rightarrow I_f^\pi)$	<i>sdf</i> -IBM	<i>spdf</i> -IBM	Expt.
$B(E2; 2_1^+ \rightarrow 0_1^+)$	180	175	142 ± 6
$B(E2; 4_1^+ \rightarrow 2_1^+)$	253	246	207 ± 4
$B(E1; 1_1^- \rightarrow 0_1^+)$	5.3×10^{-3}	2.7×10^{-4}	$\geq 1.2 \times 10^{-4}$
$B(E1; 1_1^- \rightarrow 2_1^+)$	7.5×10^{-3}	3.4×10^{-4}	$\geq 1.5 \times 10^{-4}$
$B(E1; 3_1^- \rightarrow 2_1^+)$	7.6×10^{-3}	3.7×10^{-4}	$\geq 2.2 \times 10^{-4}$
$B(E1; 3_1^- \rightarrow 4_1^+)$	5.1×10^{-3}	2.0×10^{-4}	$\geq 1.5 \times 10^{-4}$

TABLE VI. Same as the caption to Table III, but for ^{228}Ra .

$\langle I E\lambda I' \rangle$	<i>sdf</i> -IBM	<i>spdf</i> -IBM	Expt.
$\langle 2_1^+ E2 2_1^+ \rangle$	-3.3	-3.2	-0.3 ± 1.7
$\langle 4_1^+ E2 2_1^+ \rangle$	-4.3	-4.3	3.87 ± 0.19
$\langle 6_1^+ E2 4_1^+ \rangle$	5.4	5.3	5.11 ± 0.26
$\langle 8_1^+ E2 6_1^+ \rangle$	6.1	-6.0	5.89 ± 0.29
$\langle 10_1^+ E2 8_1^+ \rangle$	-6.6	6.4	7.5 ± 0.4
$\langle 3_1^- E2 1_1^- \rangle$	3.4	3.4	3.8 ± 0.5
$\langle 5_1^- E2 3_1^- \rangle$	4.6	-4.6	$3.9_{-0.8}^{+0.4}$
$\langle 7_1^- E2 5_1^- \rangle$	5.5	5.5	4.0 ± 0.9
$\langle 9_1^- E2 7_1^- \rangle$	6.1	-6.1	5.9 ± 1.0
$\langle 1_1^- E3 2_1^+ \rangle$	0.6	-0.7	1.36 ± 0.23
$\langle 3_1^- E3 0_1^+ \rangle$	-0.6	0.7	0.87 ± 0.15
$\langle 3_1^- E3 2_1^+ \rangle$	-0.7	0.7	$-0.06_{-0.16}^{+0.23}$
$\langle 4_1^+ E3 1_1^- \rangle$	-0.6	0.7	$0.4_{-1.1}^{+0.7}$
$\langle 5_1^- E3 2_1^+ \rangle$	0.9	1.0	1.71 ± 0.23

$B(E1)$ values in the *spdf*-IBM are by an order magnitude smaller than those in the *sdf*-IBM, and are of the same order of magnitude as the experimental data [47]. The $E2$ and $E3$ reduced matrix elements are listed in Table VI, in which the calculated results are compared with the recent data [48]. Apart from the sign these calculated matrix elements are mostly consistent with the experimental values.

TABLE VII. Same as the caption to Table II, but for ^{228}Th . Experimental data are from Ref. [49].

$B(E\lambda; I_i^\pi \rightarrow I_f^\pi)$	<i>sdf</i> -IBM	<i>spdf</i> -IBM	Expt.
$B(E2; 2_1^+ \rightarrow 0_1^+)$	172	165	170 ± 3
$B(E2; 4_1^+ \rightarrow 2_1^+)$	240	229	224 ± 12
$B(E2; 2_2^+ \rightarrow 0_1^+)$	0.7	1.4	1.1 ± 0.6
$B(E2; 2_2^+ \rightarrow 2_1^+)$	0.7	0.7	2.5 ± 1.4
$B(E1; 1_1^- \rightarrow 0_1^+)$	5.3×10^{-3}	3.9×10^{-4}	$(8 \pm 6) \times 10^{-4}$
$B(E1; 1_1^- \rightarrow 2_1^+)$	8.0×10^{-3}	5.9×10^{-4}	$\geq 1.4 \times 10^{-3}$
$B(E1; 3_1^- \rightarrow 2_1^+)$	7.6×10^{-3}	5.1×10^{-4}	$(3.8 \pm 0.7) \times 10^{-4}$

A measurement of the $E1$ moment was recently made for ^{228}Th [49], producing some data to be compared with the present model results. The corresponding (β_2, β_3) -PES is rather soft in β_3 deformation, but exhibits a nonzero β_3 minimum, suggesting presence of strong octupole correlations. The observed energy spectra, shown in Fig. 11, suggest the $K = 0^-$ bandhead to be in between the 4^+ and 6^+ levels, but do not appear to form an alternating-parity band. The *spdf*-IBM gives the $K = 0^-$ band that is much lower than the experimental one. The *sdf*-IBM calculation, however, reproduces the observed yrast bands of both parities rather well, and it appears that the *sdf* framework may be sufficient to account for the ^{228}Th spectra. The 0_2^+ and 2_2^+ non-yrast levels are more accurately reproduced in the *spdf*-IBM. Also, as shown in Table VII, the calculated $B(E2)$ values in the *spdf*-IBM reproduce the experimental values more accurately than the *sdf*-IBM. A significant improvement over the *sdf*-boson model is that the orders of magnitude of the calculated $B(E1)$ transition rates specifically for the $1_1^- \rightarrow 0_1^+$ and $3_1^- \rightarrow 2_1^+$ transitions are consistent with those of the experimental values.

IV. CONCLUSIONS

In the present work, dipole p boson degrees of freedom have been incorporated in the IBM mapping for describing quadrupole-octupole collective states in heavy nuclei. A procedure has been proposed that is to determine strength parameters of the *spdf*-IBM Hamiltonian using as microscopic inputs the HFB energy surfaces in terms of the axially symmetric quadrupole-octupole (β_2, β_3) , dipole-quadrupole (β_1, β_2) , and dipole-octupole (β_1, β_3) deformations. With the assumptions that some

of those parameters that appear in the *spdf*-boson model are similar to those of the *sdf* model and that most of them stay constant with nucleon number, it has been shown that one can obtain a set of the model parameters with which the IBM energy surfaces in the three deformation spaces can be made similar as much as possible to the HFB PESs, and which are physically sound in the sense that overall behaviors of the observed low-energy positive-parity and negative-parity yrast levels in the nuclei in the region of interest are reasonably described.

An illustrative application of the mapped *spdf*-IBM to axially deformed actinides $^{218-230}\text{Ra}$ and $^{220-232}\text{Th}$ revealed that the influences of including p bosons in the mapping procedure are to lower the $K = 0^-$ band, and to improve significantly the description of the observed behaviors of the $B(E1)$ values and intrinsic dipole moment with respect to the *sdf*-IBM, if the nucleon-number-dependent $E1$ transition operator that takes into account the underlying shell structure is employed. The effect of p bosons in lowering the 1^- energy level is most pronounced for those nuclei with $N \approx 132$ corresponding to the transitional region from the nearly spherical to static octupole deformed regimes. The relevant 1^- wave functions of these nuclei are accounted for by a large fraction of the p -boson configurations, which dominate over those of f bosons. For higher-spin states and states in those nuclei in the deformed region ($N \geq 134$), however, the p boson contributions are minor, and most of these states are dominated by the f -boson configurations. In these heavier nuclei, in some cases the *sdf*-IBM appears to give a sufficiently good description of the excitation energies. It was further shown that while there is essentially no significant difference between the *sdf*-IBM and *spdf*-IBM results for the $E2$ and $E3$ transition properties, the inclusion of p bosons reduces the $B(E1)$ values by orders of magnitude, which are consistent with the experimental data, in particular, for deformed heavy nuclei. The mapped *spdf*-IBM provides reasonable descriptions of the systematic of the 1^- energy levels, $B(E1; 1^-_1 \rightarrow 0^+_1)$, and $B(E3; 3^-_1 \rightarrow 0^+_1)$ values, which also compare those

of the beyond-mean-field studies starting from the same input, i.e., the constrained HFB calculations with the Gogny interactions, e.g., in Ref. [39].

Some difficulty with the model description was shown to arise in calculating the $E1$ properties of the ^{224}Ra nucleus in particular. The observed $B(E1; 1^-_1 \rightarrow 0^+_1)$ value for this nucleus is smaller than those for the neighboring isotopes by orders of magnitudes. The present *spdf*-boson model is not able to reproduce this local behavior, whereas the previous beyond-mean-field calculation [39] accounted for it. This indicates a limitation of the present version of the mapping procedure. An immediate remedy would be to devise and test in a systematic manner an $E1$ transition operator that is more realistic than that exploited here from Ref. [31]. This presents an open problem for the IBM mapping to be addressed in the future.

The *spdf*-IBM mapping procedure developed in the present study opens up several possibilities of nuclear structure studies related to octupole deformations. It will be further applied to those nuclei in other mass regions of interest in which octupole correlations are supposed to be enhanced, including the Sm-Gd nuclei in rare-earth regions, and Ba-Xe nuclei in neutron-rich lanthanides. These extended studies will allow for more accurate predictions of the spectroscopic properties of low-energy quadrupole-octupole collective states, which attract considerable attention from experimental studies using the RI beams and from the related theoretical investigations. The p -boson effects could also be relevant in the calculations of EDMs in octupole deformed odd-mass nuclei, which are of fundamental importance in basic physics. These will be interesting future studies, and related results will be reported elsewhere.

ACKNOWLEDGMENTS

This work has been supported by JSPS KAKENHI Grant No. JP25K07293.

-
- [1] P. A. Butler and W. Nazarewicz, *Rev. Mod. Phys.* **68**, 349 (1996).
 - [2] P. A. Butler, *J. Phys. G: Nucl. Part. Phys.* **43**, 073002 (2016).
 - [3] P. A. Butler, *Proc. R. Soc. A* **476**, 20200202 (2020).
 - [4] P. A. Butler, *Phys. Scr.* **99**, 035302 (2024).
 - [5] L. P. Gaffney, P. A. Butler, M. Scheck, A. B. Hayes, F. Wenander, M. Albers, B. Bastin, C. Bauer, A. Blazhev, S. Bönig, N. Bree, J. Cederkäll, T. Chupp, D. Cline, T. E. Cocolios, T. Davinson, H. D. Witte, J. Diriken, T. Grahn, A. Herzan, M. Huyse, D. G. Jenkins, D. T. Joss, N. Kesteloot, J. Konki, M. Kowalczyk, T. Kröll, E. Kwan, R. Lutter, K. Moschner, P. Napiorkowski, J. Pakarinen, M. Pfeiffer, D. Radeck, P. Reiter, K. Reynders, S. V. Rigby, L. M. Robledo, M. Rudigier, S. Sambhi, M. Seidlitz, B. Siebeck, T. Stora, P. Thoele, P. V. Duppen, M. J. Vermeulen, M. von Schmid, D. Voulot, N. Warr, K. Wimmer, K. Wrzosek-Lipska, C. Y. Wu, and M. Zielinska, *Nature (London)* **497**, 199 (2013).
 - [6] B. Bucher, S. Zhu, C. Y. Wu, R. V. F. Janssens, D. Cline, A. B. Hayes, M. Albers, A. D. Ayangeakaa, P. A. Butler, C. M. Campbell, M. P. Carpenter, C. J. Chiara, J. A. Clark, H. L. Crawford, M. Cromaz, H. M. David, C. Dickerson, E. T. Gregor, J. Harker, C. R. Hoffman, B. P. Kay, F. G. Kondev, A. Korichi, T. Lauritsen, A. O. Macchiavelli, R. C. Pardo, A. Richard, M. A. Riley, G. Savard, M. Scheck, D. Seweryniak, M. K. Smith, R. Vondrasek, and A. Wiens, *Phys. Rev. Lett.* **116**, 112503 (2016).

- [7] B. Bucher, S. Zhu, C. Y. Wu, R. V. F. Janssens, R. N. Bernard, L. M. Robledo, T. R. Rodríguez, D. Cline, A. B. Hayes, A. D. Ayangeakaa, M. Q. Buckner, C. M. Campbell, M. P. Carpenter, J. A. Clark, H. L. Crawford, H. M. David, C. Dickerson, J. Harker, C. R. Hoffman, B. P. Kay, F. G. Kondev, T. Lauritsen, A. O. Macchiavelli, R. C. Pardo, G. Savard, D. Seweryniak, and R. Vondrasek, *Phys. Rev. Lett.* **118**, 152504 (2017).
- [8] J. Engel, *Annu. Rev. Nucl. Part. Sci.* **75** (2025).
- [9] L. M. Robledo, T. R. Rodríguez, and R. R. Rodríguez-Guzmán, *J. Phys. G: Nucl. Part. Phys.* **46**, 013001 (2019).
- [10] K. Nomura, R. Rodríguez-Guzmán, Y. M. Humadi, L. M. Robledo, and J. E. García-Ramos, *Phys. Rev. C* **102**, 064326 (2020).
- [11] F. Iachello and A. Arima, *The interacting boson model* (Cambridge University Press, Cambridge, 1987).
- [12] T. Otsuka, A. Arima, F. Iachello, and I. Talmi, *Phys. Lett. B* **76**, 139 (1978).
- [13] T. Otsuka, A. Arima, and F. Iachello, *Nucl. Phys. A* **309**, 1 (1978).
- [14] J. Engel and F. Iachello, *Phys. Rev. Lett.* **54**, 1126 (1985).
- [15] J. Engel and F. Iachello, *Nucl. Phys. A* **472**, 61 (1987).
- [16] K. Nomura, D. Vretenar, and B.-N. Lu, *Phys. Rev. C* **88**, 021303 (2013).
- [17] K. Nomura, D. Vretenar, T. Nikšić, and B.-N. Lu, *Phys. Rev. C* **89**, 024312 (2014).
- [18] K. Nomura, *Int. J. Mod. Phys. E* **32**, 2340001 (2023).
- [19] K. Nomura, *Eur. Phys. J. A* **61**, 139 (2025).
- [20] M. Sugita, T. Otsuka, and P. von Brentano, *Phys. Lett. B* **389**, 642 (1996).
- [21] D. Kusnezov, *J. Phys. A: Math. Gen.* **22**, 4271 (1989).
- [22] D. Kusnezov, *J. Phys. A: Math. Gen.* **23**, 5673 (1990).
- [23] D. Kusnezov and F. Iachello, *Phys. Lett. B* **209**, 420 (1988).
- [24] N. V. Zamfir and D. Kusnezov, *Phys. Rev. C* **63**, 054306 (2001).
- [25] M. Spieker, S. Pascu, A. Zilges, and F. Iachello, *Phys. Rev. Lett.* **114**, 192504 (2015).
- [26] O. Vallejos and J. Barea, *Phys. Rev. C* **104**, 014308 (2021).
- [27] R. Bijker and F. Iachello, *Nucl. Phys. A* **957**, 154 (2017).
- [28] F. Iachello and A. D. Jackson, *Phys. Lett. B* **108**, 151 (1982).
- [29] H. Daley and F. Iachello, *Phys. Lett. B* **131**, 281 (1983).
- [30] T. Otsuka, *Phys. Lett. B* **182**, 256 (1986).
- [31] T. Otsuka and M. Sugita, *Phys. Lett. B* **209**, 140 (1988).
- [32] J. Decharge and M. Girod and D. Gogny, *Phys. Lett. B* **55**, 361 (1975).
- [33] S. Goriely, S. Hilaire, M. Girod, and S. Péru, *Phys. Rev. Lett.* **102**, 242501 (2009).
- [34] M. Kowal and J. Skalski, *Phys. Rev. C* **85**, 061302 (2012).
- [35] P. Jachimowicz, M. Kowal, and J. Skalski, *Phys. Rev. C* **87**, 044308 (2013).
- [36] A. Dobrowolski, A. Gózdź, and K. Mazurek, *Acta Phys. Pol. B* **48**, 565 (2017).
- [37] S. Kuyucak and M. Honma, *Phys. Rev. C* **65**, 064323 (2002).
- [38] R. Rodríguez-Guzmán, L. M. Robledo, and P. Sarriguren, *Phys. Rev. C* **86**, 034336 (2012).
- [39] L. M. Robledo and P. A. Butler, *Phys. Rev. C* **88**, 051302 (2013).
- [40] A. Bohr and B. R. Mottelson, *Nuclear Structure*, Vol. II (Benjamin, New York, USA, 1975).
- [41] P. Marević, N. Schunck, E. Ney, R. Navarro Pérez, M. Verriere, and J. O’Neal, *Comput. Phys. Commun.* **276**, 108367 (2022).
- [42] J. N. Ginocchio and M. W. Kirson, *Nucl. Phys. A* **350**, 31 (1980).
- [43] K. Nomura, N. Shimizu, and T. Otsuka, *Phys. Rev. Lett.* **101**, 142501 (2008).
- [44] K. Nomura, T. Otsuka, N. Shimizu, and L. Guo, *Phys. Rev. C* **83**, 041302 (2011).
- [45] D. J. Thouless and J. G. Valatin, *Nucl. Phys.* **31**, 211 (1962).
- [46] S. Heinze, computer program ARBMODEL, University of Cologne (2008).
- [47] Brookhaven National Nuclear Data Center, <http://www.nndc.bnl.gov>.
- [48] P. A. Butler, L. P. Gaffney, P. Spagnoletti, K. Abrahams, M. Bowry, J. Cederkäll, G. de Angelis, H. De Witte, P. E. Garrett, A. Goldkuhle, C. Henrich, A. Illana, K. Johnston, D. T. Joss, J. M. Keatings, N. A. Kelly, M. Komorowska, J. Konki, T. Kröll, M. Lozano, B. S. Nara Singh, D. O’Donnell, J. Ojala, R. D. Page, L. G. Pedersen, C. Raison, P. Reiter, J. A. Rodriguez, D. Rosiak, S. Rothe, M. Scheck, M. Seidlitz, T. M. Shneidman, B. Siebeck, J. Sinclair, J. F. Smith, M. Stryczyk, P. Van Duppen, S. Vinals, V. Virtanen, N. Warr, K. Wrzosek-Lipska, and M. Zielińska, *Phys. Rev. Lett.* **124**, 042503 (2020).
- [49] M. M. R. Chishti, D. O’Donnell, G. Battaglia, M. Bowry, D. A. Jaroszynski, B. S. N. Singh, M. Scheck, P. Spagnoletti, and J. F. Smith, *Nat. Phys.* **16**, 853 (2020).
- [50] H. Wollersheim, H. Emling, H. Grein, R. Kulesa, R. Simon, C. Fleischmann, J. de Boer, E. Hauber, C. Lauterbach, C. Schandera, P. Butler, and T. Czosnyka, *Nucl. Phys. A* **556**, 261 (1993).
- [51] P. Butler and W. Nazarewicz, *Nucl. Phys. A* **533**, 249 (1991).
- [52] M. Spieker, D. Bucurescu, J. Endres, T. Faestermann, R. Hertzenberger, S. Pascu, S. Skalacki, S. Weber, H.-F. Wirth, N.-V. Zamfir, and A. Zilges, *Phys. Rev. C* **88**, 041303 (2013).